

Simulation of Large-Scale Tunnel Belt Fire and Smoke Characteristics under a Water Curtain System Based on CFD

Yinuo Chen, Jinzhang Jia,* and Guangbo Che*



Cite This: *ACS Omega* 2022, 7, 40419–40431

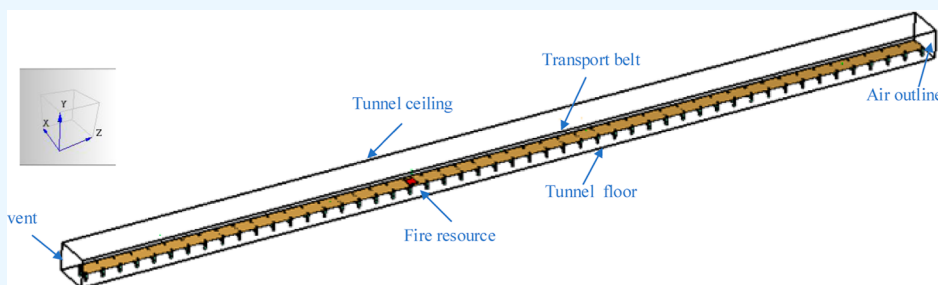


Read Online

ACCESS |

Metrics & More

Article Recommendations



ABSTRACT: Transport belt fires pose a serious threat to the lives of miners. The smoke spread characteristics of transport belt fires are important for the effective construction of underground safety works. In this paper, a water curtain system is added to ventilation to investigate the effectiveness of water spray in blocking fire-induced smoke and heat. Using computational fluid dynamics (CFD) simulations obtained with FDS 6.0.1, full-scale underground belt transport tunnel fire tests are conducted with mechanical ventilation and a water curtain system to obtain smoke spread characteristics, temperature distribution, visibility profiles, and CO distribution. The results show that the addition of a water curtain system can effectively limit temperature and smoke, but high mechanical ventilation velocities are not conducive to the water curtain system, limiting underground tunnel fires. This study found that the mechanical ventilation velocity should be controlled at approximately 0.8 m/s when the water curtain system is on a 100 m beltway. Smoke across the water curtain system area, smoke stratification in the lower layer of the water curtain area is lost, the water curtain system in the lower layer of the tunnel will affect the flow field and temperature field flowing to the fire source, and the blockage effect is the most obvious in the upper layer of the tunnel. The water curtain system reduces the distribution of temperature and CO concentration in the tunnel and rapidly restores visibility. With the addition of the water curtain system, the environment in the restricted area is suitable for occupant evacuation and firefighting, and the system can be considered a viable strategy for tunnel smoke control.

1. INTRODUCTION

With the increased exploitation of underground space in mines, tunnels, subways, underground warehouses, and underground shopping malls, the frequency of fire accidents is increasing and is causing increasing concern worldwide.¹ Mine fires not only burn large amounts of resources, materials, and production equipment but also freeze the recoverable reserves of coal and severely disrupt normal production due to the closure of the fire area; burning consumes oxygen in the air, causing the concentration of oxygen in the air flow to drop while generating large amounts of harmful heat, toxic and hazardous gases, and dust, causing burns, poisoning, or suffocation of underground personnel. For example, the 2006 underground mine conveyor belt fire at the Aracoma Alma no. 1 mine in Logan County, West Virginia, resulted in fatal injuries to two miners when they were separated from their navigator while attempting to escape the fire.

Belts can cause fires when operated in mine belt tunnels. Toxic gases and smoke from burning belts spread into the tunnels with wind currents, exposing miners to toxic and hazardous gases such as CO, HCL, SO₂, H₂S, and NO_x. At the same time, the smoke from burning belts limits visibility, which makes it more difficult for workers to escape from the mine. As a result, many studies have been conducted on underground fires, both nationally and internationally, to reduce underground personnel exposure to high temperatures and toxic and hazardous gases during evacuation.

Received: August 24, 2022

Accepted: October 19, 2022

Published: October 28, 2022



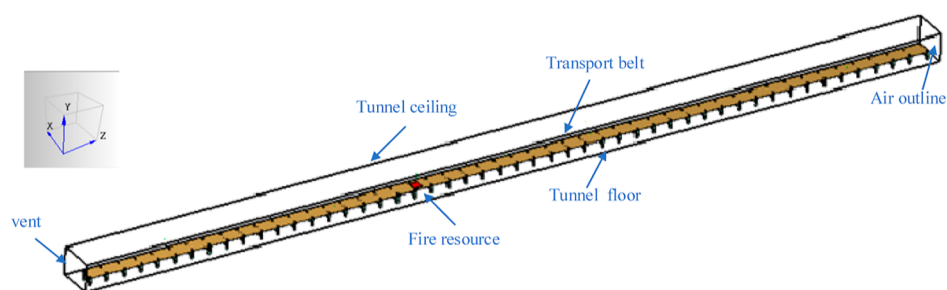


Figure 1. Geometry of the underground belt tunnel.

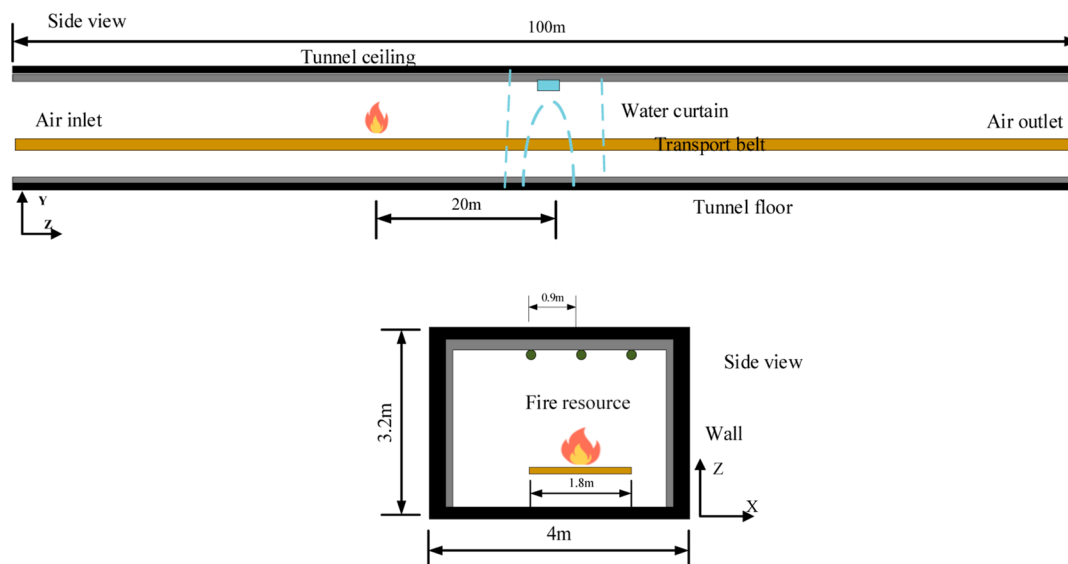


Figure 2. Side views of the coal mine in an underground transport belt tunnel.

Most studies initially focused on smoke movement, smoke stratification, and smoke temperature due to underground fires, which were investigated through scaled-down experiments and mathematical models of underground spaces.^{2–5} These studies established empirical equations for the stratification of flue gas return flows and models for the stratified motion of hot gases in confined spaces. In addition, researchers have come to realize that ventilation systems play a crucial role in influencing smoke movement and can be used to control smoke in tunnels. Hu et al. conducted a series of studies on the characteristics of tunnel flue gas temperature distribution and CO distribution under different ventilation rates and deduced the backflow length formula of flue gas.^{6–10} Fan et al. used numerical simulation methods in underground spaces to optimize ventilation schemes for smoke extraction efforts.¹¹

In recent years, researchers have also introduced water curtain systems to control underground fires and smoke flow and temperature distribution. Amano et al. and Murakami et al. proposed the addition of a water curtain spray system to tunnels.^{12,13} A special arrangement of 200 μm -diameter nozzles was used to form a fire compartment to prevent smoke spread and heat propagation. Ingason carried out a 1:23 scale model tunnel study to improve the basic understanding of water jetting systems in longitudinal tunnel flows.¹⁴ McCorry proposed the addition of lateral ventilation to a water curtain system to collectively extract smoke from underground spaces. Smoke can be quickly removed from restricted areas to ensure the safe evacuation of workers.¹⁵ Liang et al. investigated the interaction between lateral ventilation and water curtains in large-scale

tunnels.¹⁶ The study showed that a combination of water curtain and lateral ventilation systems can effectively confine fire and smoke, while the environment within the restricted area is suitable for occupant evacuation and firefighting. Although most studies have demonstrated that water curtain systems can contain the spread of fire, the characteristics of smoke movement will change because of the reduced buoyancy caused by the flow caused by the addition of water mist and cooling with the water mist. This causes a drop in smoke in localized spray areas, which reduces the visibility of evacuees located within the spray area and hinders their evacuation. Sun et al. tested a fine water mist system for stopping fire-induced smoke and heat in reduced tunnels where longitudinal ventilation was present or not. The results confirmed that the water system was effective in reducing temperatures and preventing the spread of smoke in the absence of longitudinal ventilation.¹⁷ Li et al. investigated the effectiveness of a fine water mist tube sheet system in blocking fire-induced smoke and heat using a 1/3 scale model tunnel fitted with a fine water mist tube sheet system. The phenomenon of smoke obstruction caused by the fine water mist tube section system was discussed and explained based on the temperature distribution in the model tunnel.¹⁸

In the studies mentioned above, scholars have primarily focused on discovering the distribution of smoke and temperature caused by ventilation systems or water curtain systems using reduced scale experiments and CFD methods. Few studies have addressed scenarios where water spray systems are combined with ventilation systems in underground belt tunnel fires in coal mines. This paper uses the fire dynamics simulator

(FDS) to analyze the flow and temperature fields in detail to better elaborate and explain the water spray, ventilation, and fire-induced smoke vortex motion. In addition, this paper investigates the temperature distribution, visibility, and CO concentration distribution in a tunnel after an underground belt fire in a coal mine, which has important implications for underground fire prevention and control, as well as for underground disaster avoidance and rescue.

2. SIMULATION METHOD

2.1. Physical Model. Due to the complex site layout of the coal transport belt tunnel and the presence of belt conveyors, cables and wires, fire hoses, belt ladders, and other equipment, it is difficult to establish a model that is identical to the real-world conditions and to simplify assumptions about secondary factors for the transport belt tunnel. The geometric structure of the underground coal mine belt tunnel, as shown in Figure 1, was established. Based on the actual situation of coal transport belt tunnel production in coal mines, the dimensions of the tunnel were established as 100 m long \times 4 m wide \times 3.2 m high. The left side of the tunnel is a footpath, which is an emergency escape route in the case of fire, and the conveyor is located in the middle of the tunnel on the right side, with its transport mode being head unloading and tail receiving. In the physical model, the tunnel walls are made of concrete with a thickness of 0.5 m and a thermal conductivity of 1.8 W/(M·K).

Figure 2 shows a side view of the transport belt tunnel, showing the location of the fire source, transport belt, ventilation openings, and water curtain nozzles. The fire source is located in the center of the transport belt with a power size of approximately 3.35 MW. The transport belt width is 1.8 m, and the surface is 1 m from the tunnel floor. The distance from the left side of the transport belt edge to the tunnel wall is 1.5 m, and the distance from the right side of the transport belt edge to the tunnel wall is 0.7 m. The thermal conductivity of PVC is 0.14–0.17 W/(M·K). Both ends of the tunnel are open, and the left end of the tunnel is set as the air inlet. The right end of the tunnel is the air outlet, and the ambient temperature is 20.0 °C. The water curtain system consists of three rows of nozzles, with each nozzle set to have a flow rate of 30 L/min, an initial velocity of 50 m/s, a particle size of 120 μ m, a nozzle pressure of 10 MPa, and a droplet mass flux of 0–0.75 kg/m²/s. In addition, this research also considers obstacles such as fire extinguishing boxes and bearing columns, which will affect the smoke within the area, to bring the simulation closer to the real situation.

2.2. Fire Model. The fire dynamics simulator (FDS) was developed by the National Institute of Standards and Technology (NIST).²² It has become one of the most widely used CFD software for simulating engineering fluid flows. FDS can solve Navier–Stokes equations for fire-induced, low-velocity, thermally driven flows and heat transfer. In this study, FDS version 6.7.1 was used to study fires in urban underground utility tunnels. The LES model was chosen to calculate the smoke flow and radiative heat transfer processes during the simulation of combustion under a water curtain.

The conservation of mass formula is defined as

$$\frac{\partial \rho}{\partial t} + \nabla \cdot (\rho u) = 0 \quad (1)$$

where u is the velocity vector, m/s, and ρ is the gas density, kg/m³.

The component equations are defined as

$$\frac{\partial \rho}{\partial t} (\rho Y_L) + \nabla \cdot \rho Y_L u = \nabla \cdot (\rho D)_L \nabla Y_L + \dot{m}''' \quad (2)$$

where Y_L is the mass fraction of substance L; D is the diffusion coefficient, m²/s; and \dot{m}''' is the production rate per unit volume of substance L, kg/s/m³.

The kinetic energy equation is defined as

$$\rho \left(\frac{\partial u}{\partial t} + (u \cdot \nabla) u \right) + \nabla p = \rho g + f + \nabla \cdot \tau \quad (3)$$

where τ is the viscous pressure vector, kg/s²/m; g is the acceleration of gravity, m/s²; and f is the external force vector (excluding gravity), kg/s²/m.

The energy equation is defined as

$$\frac{\partial}{\partial t} (\rho h) + \nabla \cdot \rho h g - \frac{Dp}{Dt} = \dot{q}''' - \nabla \cdot q_r + \nabla \cdot k \nabla T + \nabla \cdot \sum_1 h_1 (\rho D)_1 \nabla Y_1 \quad (4)$$

where q_r is the radiant heat flux, KW/m²; h is the enthalpy, KJ; k is the thermal conductivity, W/m/K; and \dot{q}''' is the heat release rate per unit volume, KW/m³.

The Rosin–Rammler–Lognormal distribution was used to characterize the Lagrangian particle size distribution, and the particle body accumulation fraction (CVF) relationship is defined as

$$F(d) = \begin{cases} \frac{1}{\sqrt{2\pi}} \int_0^d \frac{1}{\sigma d'} e^{-[\ln(d'/d_m)]^2 / 2\sigma^2} dd' & (d \leq d_m) \\ 1 - e^{-0.693 \left(\frac{d}{d_m}\right)^\gamma} & (d > d_m) \end{cases} \quad (5)$$

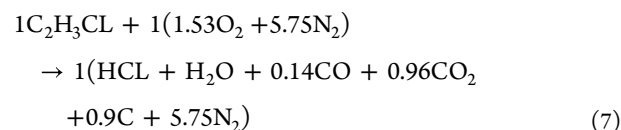
where d_m is the diameter of the particles and γ and σ are empirical parameters.

FDS takes into account the attenuation of thermal radiation by droplets through scattering and absorption, which is important in fine water mist environments. Under simplified conditions ignoring gas phase absorption and radiative heat radiation, the heat radiation equation is

$$\vec{s} \cdot \nabla I_{\vec{s}}(x, \vec{s}) = -[k_d(x, \lambda) + \sigma_d(x, \lambda)] I_{bd}(x, \vec{s}) + \frac{\sigma_d(x, \lambda)}{4\pi} \int_{4\pi} \Phi(\vec{s}, \vec{s}') I_{\vec{s}'}(x, \vec{s}') ds' \quad (6)$$

where k_d and σ_d are the absorption coefficient and scattering coefficient of the liquid particle, respectively, $I_{bd}(x, \lambda)$ represents the emission term of the particle, and $\Phi(\vec{s}, \vec{s}')$ is the scattering phase function, giving the radiation intensity from the \vec{s}' to \vec{s} direction.

2.3. PVC Combustion Response. The structure of flame-retardant conveyor belts currently used in coal mines in China is mainly divided into two categories: fabric fiber core and steel wire rope core. The material wrapping and covering the core is mainly polyvinyl chloride plastic (PVC). Therefore, in this study, the ignition source is set as the PVC material, and its combustion reaction equation is as follows



according to formula (7), the reactants and products are defined in FDS, and the relevant parameters are set to simulate.

2.4. Sensitivity Study on the Grid System. The appropriate grid size directly determines the accuracy of the FDS simulation results. Usually, a larger grid size will lead to faster convergence; however, this will reduce the quality of model testing to some extent, while a smaller grid size will lead to slower convergence but higher quality prediction results.^{19,20} Therefore, considering the balance between simulation accuracy and computational cost, it is necessary to find a suitable grid through grid size optimization.²¹ In this paper, five different grid sizes were selected for the simulation, as detailed in Table 1.

Table 1. Details of Five Different Mesh Sizes: 0.2, 0.175, 0.15, 0.125, and 0.1 m

grid system	size of the grid	total cell number
I	0.2 m × 0.2 m × 0.2 m	160,000
II	0.175 m × 0.175 m × 0.175 m	241,200
III	0.15 m × 0.15 m × 0.15 m	400,890
IV	0.125 m × 0.125 m × 0.125 m	665,600
V	0.1 m × 0.1 m × 0.1 m	1,280,000

In this study, temperature and visibility are important parameters for characterizing smoke dispersion, and temperature, visibility, and CO distribution are important factors for assessing the conditions for maintaining the evacuation of people in a fire.^{20,22–24} Therefore, the relationship between grid size and calculation results was analyzed through the distribution of temperature, visibility, and CO concentrations in belt transport tunnels with different grid sizes.

The simulation results for temperature, visibility, and CO concentration for different grid sizes are shown in Figure 3. We find roughly the same trend for the five grid types. In Figure 3a, when the grid size is larger, the calculated temperature increases, which indicates that the simulation results for temperature are higher if the grid size is too large.^{26,27,29} In Figure 3b,c, as the simulation grid size increases, the visibility decreases and the CO concentration increases. The abovementioned five grid sizes indicate that finer grids will give more accurate results. The simulation results for larger grid sizes have lower accuracy but again reflect the trend of the parameters. The grid sizes in Figure 3a–c are 0.1 m, 0.125 m, and 0.15 m. The results for temperature, visibility, and CO concentration are not significantly different for a grid size of 0.15 m, that is, a finer grid size does not optimize the results too much.

This paper assesses the quality of the grid size predictions by looking at the vortices formed by the smoke.^{25,29} Figure 4 illustrates the velocity vortices for five different grid sizes. It can be observed that the difference in vorticity between grid system I, II, and III simulations near the fire source is not significant, while grid system IV and V simulations near the fire source show significant vortex folds, although grid system V has a finer grid division compared to the other four grid systems. This means that grid system V takes more time to calculate, while its simulation results have a slight improvement in accuracy. Therefore, based on the results of the appeal grid sensitivity analysis, this paper uses grid system IV for the simulations, setting the grid system IV grid size to 0.15 m × 0.15 m × 0.15 m and the total grid number to 400,890.

2.5. Simulation Cases. To study the heat insulation and smoke resistance effect of the water curtain system, four fire conditions are selected in this paper, as shown in Table 2. The

water curtain system is set on the right side of the fire source, and the water curtain system and mechanical ventilation work together to suppress the temperature increase and the smoke spread.

This paper is a study of the influence of ventilation and water curtain systems on smoke control and evacuation of people from underground transport belt fires. The smoke propagation of transport belt fires under different working conditions is analyzed by studying important parameters such as the velocity field, temperature, and visibility of the fire. The state of smoke movement depends heavily on the movement of hot air, so temperature distributions are modeled to indicate smoke propagation at various locations.²⁰

Ultimately, three horizontal slices ($Y = 1.5$ m, $Y = 1.8$ m, and $Y = 2.6$ m) are defined in this paper, where $Y = 1.5$ m is used to compare and analyze the toxic and hazardous gas concentration and visibility distributions, and $Y = 1.5$ m, $Y = 1.8$ m, and $Y = 2.6$ m are used to analyze the temperature and velocity fields. On the one hand, because the usual height of the human eye is between 1.2 and 1.8 m, heights of 1.5 and 1.8 m for the human eye were used.^{28,29} On the other hand, because the roof temperature of the tunnel also plays an important role in fire analysis, a tunnel roof height of 2.6 m was used.

3. RESULTS AND DISCUSSION

3.1. Shielding Efficiency of Different Ventilations under Water Curtain Systems. To evaluate the thermal insulation effect of the water curtain system, the thermal insulation efficiency is used to characterize the ability of the water curtain to attenuate the heat radiation from a fire. Thermal insulation efficiency is defined as the difference between the temperature of the same point before and after the separation of the water curtain ($T_1 - T_2$) and the temperature of the point without the separation of the water curtain (T_1). The formula is expressed as

$$\eta = \frac{T_1 - T_2}{T_1} \times 100\% \quad (8)$$

where T_1 is the temperature of the measurement point when the water curtain is not activated, in °C, and T_2 is the temperature of the measurement point when the water curtain is activated, in °C.

Figure 5 shows the thermal insulation effect of the water curtain with four ventilation speeds of 0, 0.8, 1.2, and 1.5 m/s and the water curtain system working together. The water curtain insulation effect is mostly concentrated in the 30–70% stage. However, the greater the ventilation speed is, the better the thermal insulation effect with the water curtain system. In this study, when the ventilation speed is 0.8 m/s, the water curtain system has the best thermal insulation effect; when the ventilation speed is 1.2 m/s, the thermal insulation effect is second, and when the ventilation speed is 0 and 1.5 m/s, the thermal insulation effect is poor. Therefore, the main research approach is to study the effect of heat and smoke insulation with the water curtain system when the ventilation speed is 0.8 m/s.

3.2. Distribution of Temperature under the Water Curtain System. Figure 6 shows the longitudinal cross section for case 4 at $X = 1.6$ m for simulation times of 10, 20, 50, 100, 200, 400, and 600 s. As shown in Figure 6, the belt burned sufficiently to spread rapidly to the ends of the tunnel due to the abundance of oxygen in the underground tunnel. The main reason for this phenomenon is that the gas diffusion to the right

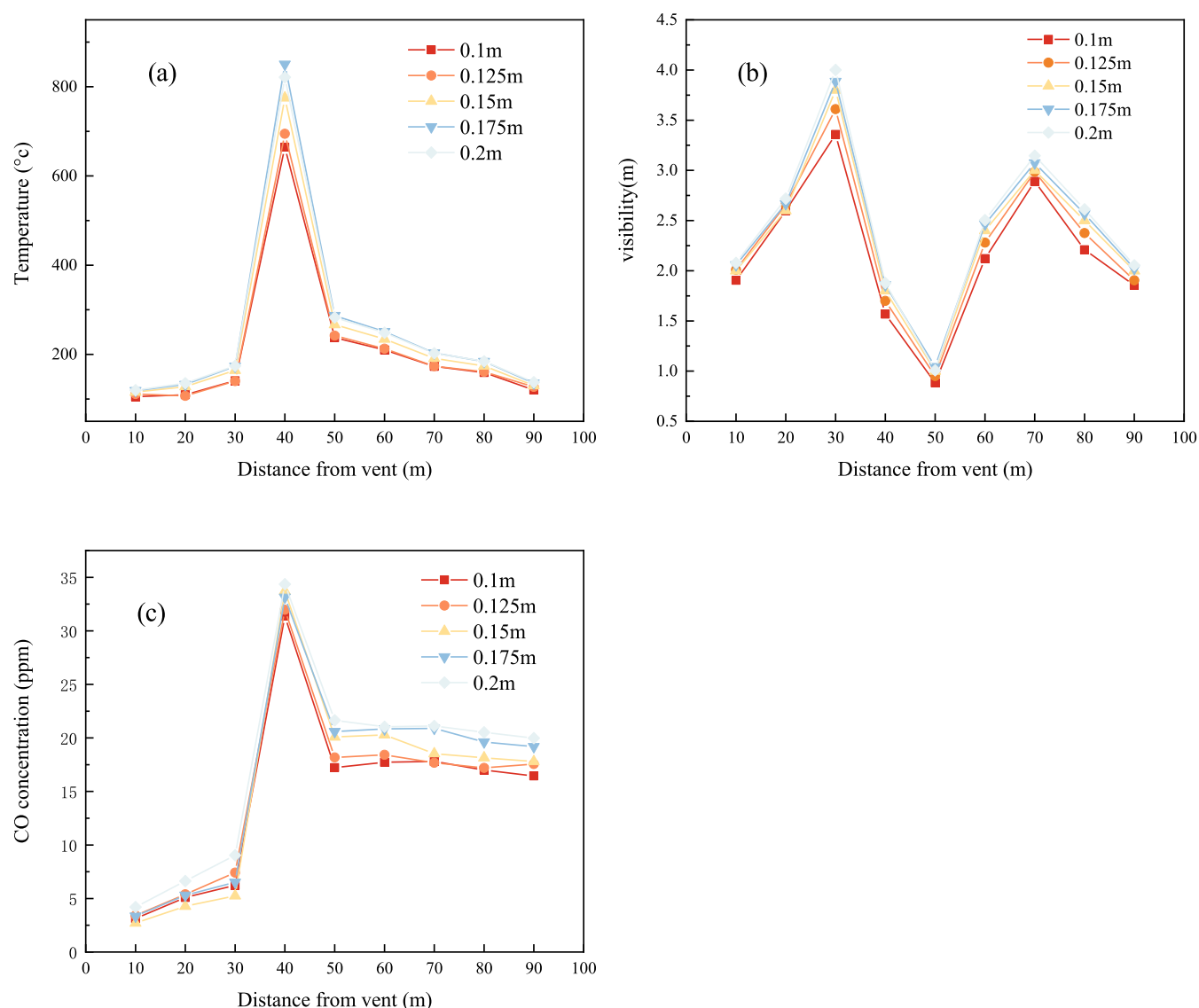


Figure 3. Three-parameter comparison for different grid systems at a simulation time of 300 s: (a) comparison of temperature at $X = 1.6$ m; (b) comparison of visibility at $X = 1.6$ m; and (c) comparison of CO concentration at $X = 1.6$ m.

end of the tunnel is greater because the left side of the tunnel is ventilated, while the gas diffusion to the left end of the tunnel is weaker. When the time reaches 20 s, the fire becomes larger and gradually spreads to both ends of the tunnel as the burning area expands. At the same time, the smoke rises vertically under the buoyancy of the heat plume from the fire source, and as the wind is blowing to the right, the visibility of the right-hand side of the tunnel rapidly decreases, and the smoke spreads to both ends, with the upwind side of the tunnel having good visibility for the first 20 m of the tunnel due to ventilation. Visibility is the distance at which an observer can identify an object relative to the background, taking 10 m as the fire hazard critical value.²⁰ When the time reaches 100 s, the fire tends to stabilize, and the underground belt transport tunnel is gradually filled with smoke, resulting in very low visibility, which then shows a stratified state under the upper mold, with the visibility of the upper layer being lower than that of the lower layer. When the time reaches 400 s, the smoke completely fills the tunnel, and the visibility range tends to stabilize. Therefore, the next part of this study focuses on the changes in the fire after the addition of the water curtain system during the 200–400 s period of fire stabilization. Finally,

the intensity of PVC burning gradually decreases as oxygen is consumed.

An enlarged view of the water spray area of the water curtain is shown in Figure 7. It can be seen that the jet produced by the water spray from the sprinkler drags the smoke flow from the fire side and the fresh air from the outside. This mixture is then projected onto the ground, creating a cooling plume of smoke that flows sideways. However, due to the entrainment caused by the jet, the smoke is not completely blocked by the water mist curtain. The streamlines in Figure 7 clearly demonstrate this.

3.2.1. Distribution of the Flow Field under the Water Curtain System. Figure 8 shows the temperature field (left) and longitudinal velocity component (right) in the vertical mid-plane ($y = 1.6$ m) with the addition of the water curtain system during the fire stabilization period (200–400 s). The temperature profile in the figure (left) shows the composite flow of the fire and smoke plume obstructions for the longitudinal ventilation flow at $z = 40$ m (center of the fire source) and $z = 60$ m (location of the water curtain system). With the increase in the number of water jets, the fluctuation of the composite flow tends to be smooth and the propagation range decreases. The

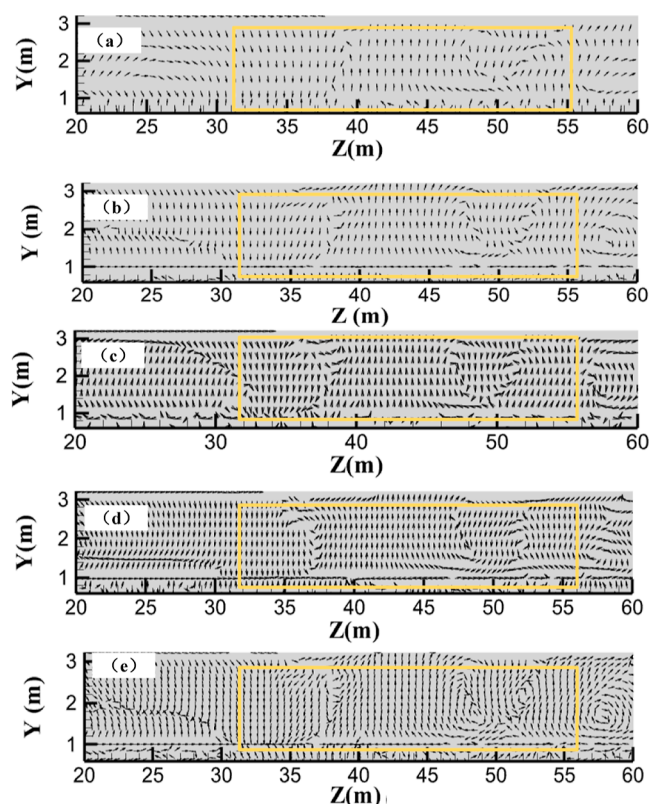


Figure 4. Velocity vectors near the fire source at a simulation time of 150 s: (a) grid system I; (b) grid system II; (c) grid system III; (d) grid system IV; and (e) grid system V.

Table 2. Summary of Different Simulation Cases

case	situation
1	ventilation 0 m/s + water curtain system
2	ventilation 1.2 m/s + water curtain system
3	ventilation 1.5 m/s + water curtain system
4	ventilation 0.8 m/s
5	ventilation 0.8 m/s + one row of water curtain
6	ventilation 0.8 m/s + two rows of water curtain
7	ventilation 0.8 m/s + three rows of water curtain

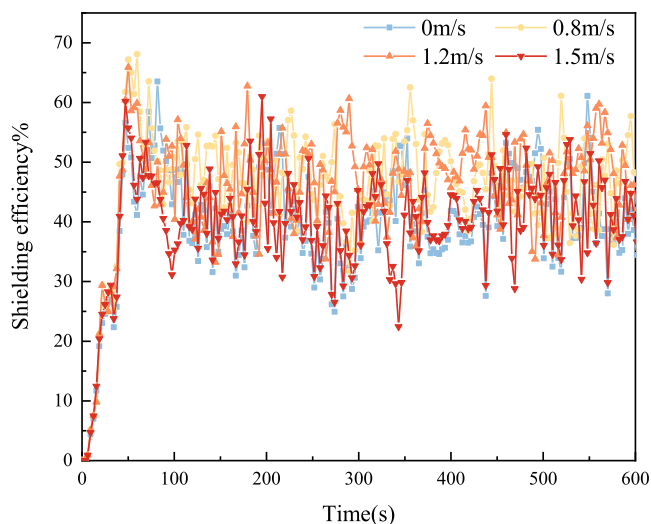


Figure 5. Shielding efficiency under four different ventilations.

main purpose of this paper is to analyze the effect of water spray on the velocity and temperature fields in more detail. Therefore, we focus on this area ($z = 40$ m and $z = 60$ m).

By observing the horizontal velocity component (V), it is found that when there is no water spray (a), the velocity close to the flame is the largest, but the incoming wind speed in the tunnel due to the effect of thermal buoyancy changes the direction of the flow velocity, which affects the area behind the flame (65–100 m). Flow velocity has little effect. There is a large-scale vortex structure in the direction of the velocity vector near the flame. The longitudinal ventilation and the air outside the flame flow to the flame area under the action of the pressure gradient. Under the action of the flame and the surrounding shear force, the flow direction is changed, resulting in a large-scale vortex. At the same time, it is worth noting that as the fire developed, a large number of vortex structures were also generated in the rear area of the figure. From the direction of the velocity vector, it can be seen that the vortex is a wake vortex structure generated by the incoming air in the pipe around the flame. In the horizontal velocity component (V) of the water curtain system (b), (c), and (d), with the increase in the number of water jets, the thermal buoyancy is reduced, the increase in the fluid mass flow velocity is weakened, and the increase in the flow velocity of the fluid mass is delayed. Vortex generation.

Figure 9 shows the vertical velocity components (left) and longitudinal velocity components (right) near the height of the transport belt ($Y = 1.5$ m) during the fire stabilization period (200–400 s). Looking at the vertical velocity vector W (left), it can be seen that in the area of the fire ($Z = 40$ –60 m), the left side of the vertical middle plane has a greater velocity and tends to flow more due to the “push” effect of the hot smoke (left to right flow).

Looking at the horizontal velocity vector V (right), the vortex is most pronounced in case (a) and very confused in case (d), indicating that the vortex formation velocity decays as the number of spray rows increases. This is due to the upward movement of the droplets between the rows of spray. The flow caused by the spray hits the floor of the tunnel, creating a “push” force that causes the cold air in the area to flow upward, reducing thermal buoyancy, attenuating the flow velocity, and delaying the creation of vortices. This is a complex flow process that carries water mist and combines it with fire (smoke)- and ventilation (air)-induced flow in a horizontal direction.

Figure 10 shows the vertical velocity component (left) and longitudinal velocity component (right) at the height of the tunnel ($Y = 1.8$ m) during the fire stabilization period (200–400 s). The vertical flow velocity W (middle) in the tunnel becomes increasingly complex, showing a trend of smoke pushing to the right. When $Y = 1.8$ m, the vertical flow velocity stratification of each condition decreases compared to $Y = 1.5$ m, and the flow field within the vertical velocity vector of all conditions is stable with increasing height. The rate of vortex formation in the horizontal velocity vector V (right) decays with an increasing number of water spray rows.

Figure 11 shows the vertical velocity components (left) and longitudinal velocity components (right) near the height of the roof ($Y = 2.6$ m) during the fire stabilization period (200–400 s). Looking at the vertical velocity vector W (middle), the extent that as the number of rows of water curtain increases, the velocity on the right side of the flame increases, the flow pattern on the left side of the flame becomes more complex, and the right side of the fire source shows a tendency to push to the left. This effect is similar to the vertical velocity vector W in Figures 9

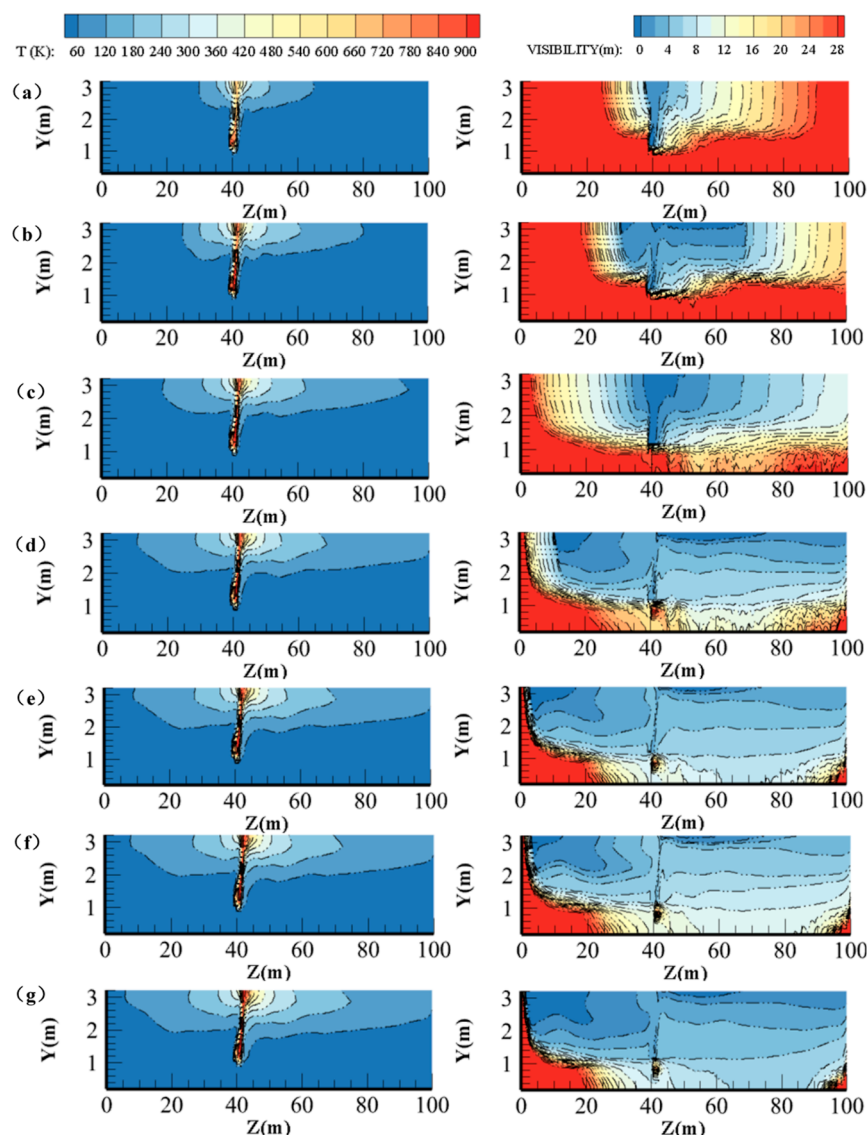


Figure 6. Temperature and visibility contours (no spray) at the section of $X = 1.6$ m in case 4 at different simulation times, (a) $t = 10$ s, (b) $t = 20$ s, (c) $t = 30$ s, (d) $t = 100$ s, (e) $t = 200$ s, (f) $t = 400$ s, and (g) $t = 600$ s.

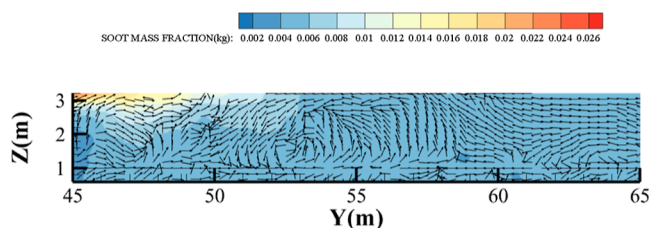


Figure 7. Simulate a contour plot of the soot mass fraction with streamlines (arrows showing the location of the injection).

and 10, but because the smoke has more horizontal momentum near the top plate, the horizontal flow has not yet been biased to flow vertically downward, the flow velocity of the water curtain is greater than the flow velocity of the smoke, and smoke blockage occurs.

Looking at the horizontal velocity vector V (right), in the case without water spray (a), the vortex structure is very pronounced, which is generated around the fire source due to thermal buoyancy and ventilation. In cases (b), (c), and (d), when the water curtain system is added, the vortex becomes less

pronounced and is generated over a greater distance and at a slower speed. This is due to the upward flow between the rows of droplets, which will be entrained into the water spray and the impingement, hindering the thermal buoyancy and the velocity of the vortex generated by the ventilation, that is, the push of the smoke from the left to the right side. This impact effect of upward flow between sprays helps to block smoke propagation. The greater the number of rows of water curtains, the more upward impingement between sprays and the more significant the blocking effect.

3.2.2. Temperature Distributions. Figure 12 shows a quantitative comparison of simulation results at three levels for tunnel fires in the case of a no-water curtain system (left) and a three-drainage curtain system (right). The water curtain system starts after 40 s, where $Z = 20$ m is located upstream of the fire source and the water curtain system, $Z = 50$ m is located downstream of the fire source and upstream of the water curtain system, and $Z = 80$ m is located downstream of the fire source and water curtain system. The temperature curve at $Z = 20$ m shows that under ventilation of 0.8 m/s, the activation of the

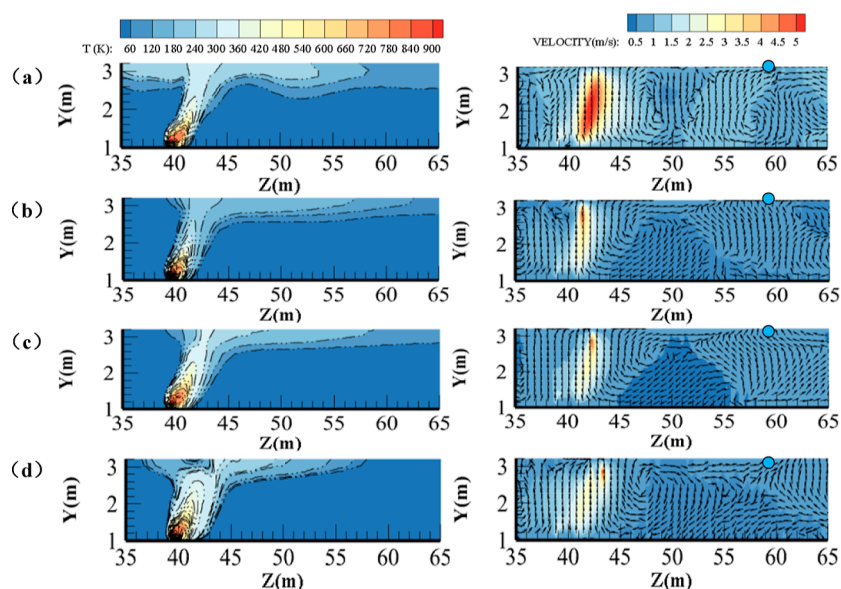


Figure 8. Temperature field (left) and longitudinal velocity component (right) of the simulated water curtain system. (a) No spray, (b) one row of water spray, (c) two rows of water spray, and (d) three rows of water spray. At the vertical plane ($x = 1.6$ m), values have been averaged over the steady-state period (200–400 s).

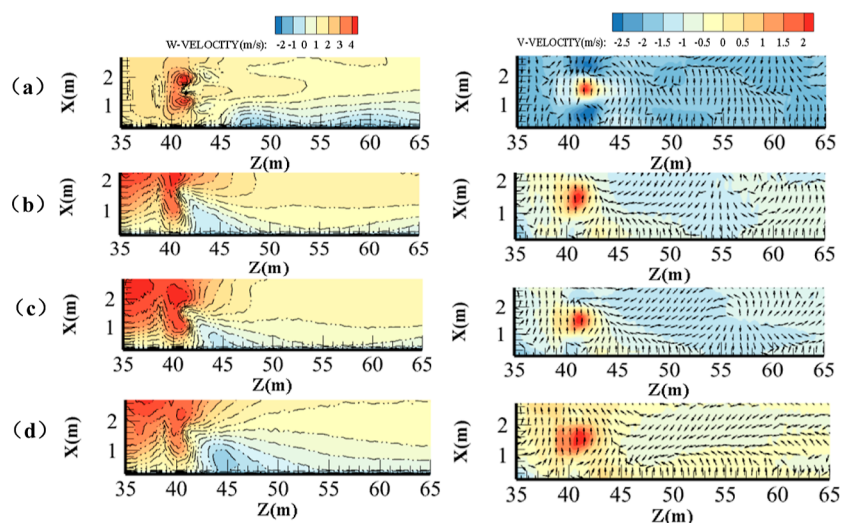


Figure 9. Temperature field (left), vertical velocity component (middle), and longitudinal velocity component (left) of the simulated water curtain system. (a) No spray, (b) one row of water spray, (c) two rows of water spray, and (d) three rows of water spray. In the vertical plane ($Y = 1.5$ m), the values were averaged over the steady-state period (200–400 s).

water curtain system has little effect upstream of the fire source ($Z = 20$ m). However, the activation of the water curtain system at $Z = 50$ m and $z = 80$ m downstream from the fire source will have some effects. The effect of water spray at the position $Z = 50$ m is greater than that at the position $Z = 80$ m, and the cooling effect is more obvious because the effect of water spray on the flame flow field at a close range is greater. It can also be observed that the temperature near the roof of the tunnel at $Y = 2.6$ m is much higher than that in the middle layer of the tunnel at $Y = 1.5$ m and $Y = 1.8$ m, and the upstream of the water curtain system hardly affects the smoke stratification. Combining Figures 8, 9, and 10, it is worth noting that at the position of the fire source, the presence of water spray to the upper layer is more obvious. The pushing effect of the airflow becomes increasingly obvious with increasing height, which can be seen in

the temperature field and velocity field of the horizontal plane. When $Y = 2.6$ m, the blocking effect is the most obvious.

Figure 13 shows the distribution of temperature in the horizontal section at the height of the tunnel ($Y = 1.5$ m) during the fire stabilization period (200–400 s). These figures show that the high-temperature zone is located in the 35–45 m area, the highest temperature without water spraying. When the water curtain system is activated, the increase in the number of water curtain rows has a lowering effect on the temperature. When water is sprayed from three rows, the temperature inside the tunnel is the lowest. Smoke spread at $Z = 30$ m and $Z = 50$ m is blocked, compared with the no water spraying case when the smoke layer temperature is reduced, the high-temperature zone is confined within the water curtain screen, and the temperature outside the fire area is close to the ambient temperature.

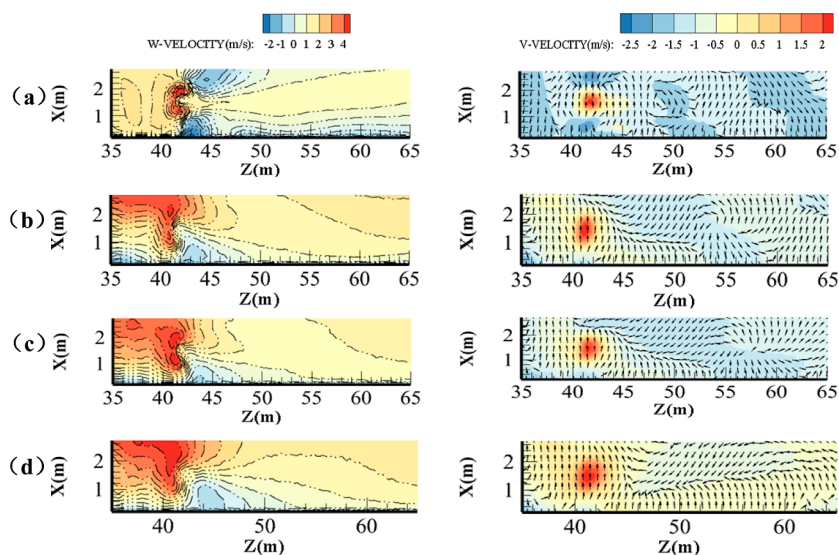


Figure 10. Vertical velocity component (left) and longitudinal velocity component (right) of the simulated water curtain system. (a) No spray, (b) one row of water spray, (c) two rows of water spray, and (d) three rows of water spray. In the horizontal plane ($Y = 1.8$ m), the values have been averaged over the steady-state period (200–400 s).

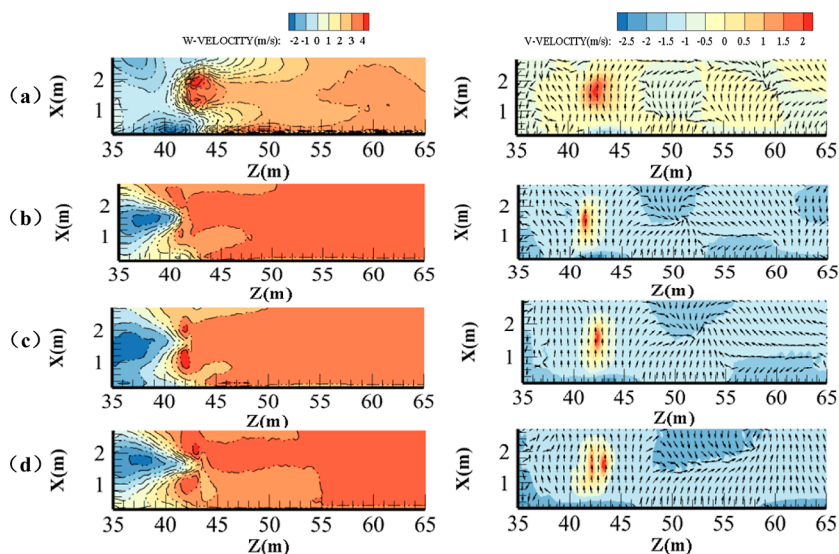


Figure 11. Temperature field (left), vertical velocity component (middle), and longitudinal velocity component (left) of the simulated water curtain system. (a) No spray, (b) one row of water spray, (c) two rows of water spray, and (d) three rows of water spray. In the vertical plane ($Y = 2.6$ m), the values were averaged over the steady-state period (200–400 s).

3.3. Distribution of Visibility and Concentration under the Water Curtain System. 3.3.1. Visibility Distributions.

Visibility is one of the important parameters in fire safety assessment. Figure 14 shows the visibility contours near the fire source at the longitudinal section ($X = 1.6$ m) during the fire stabilization phase (200–400 s). It can be observed that in cases (b), (c), and (d), the visibility near the fire source is truncated by eddies due to the increased efficiency of the water mist in flushing the smoke particles after the addition of the water curtain system, which has a significant smoke stopping effect and creates an area inside which the visibility cannot be greatly improved. This is due to the increased momentum of the smoke and water mixed flow; when the impact on the ground after the rebound effect is obvious, the rebound of the airflow back up results in a reduction in visibility rebound rate. As the number of water curtain rows increases, the thermal buoyancy and droplet gravitational acceleration around the effect of the flow in a vortex

impede the propagation of smoke and improve visibility inside the tunnel. The visibility near the water curtain increases to 16 m, which is improved in the visibility comparison case (a) after the tunnel $Z = 80$ m, that is, outside the confined area, visibility is high, which indicates that the system can be used to effectively limit the propagation of smoke.

Figure 15 shows the visibility contours of the horizontal section at human eye height ($Y = 1.5$ m) during the simulation time in the fire stabilization phase (200–400 s). In the no spray case, the vast majority of the tunnel was found to have visibility below 6 m, which is very dangerous for evacuation and rescue, except in small areas away from the fire source. In other cases, the visibility in the tunnel increased as the number of water spray rows increased.

3.3.2. CO Concentration Distributions. Figure 16 shows the distribution of CO gas concentrations in the tunnel at the longitudinal section ($X = 1.6$ m) at the simulation time during

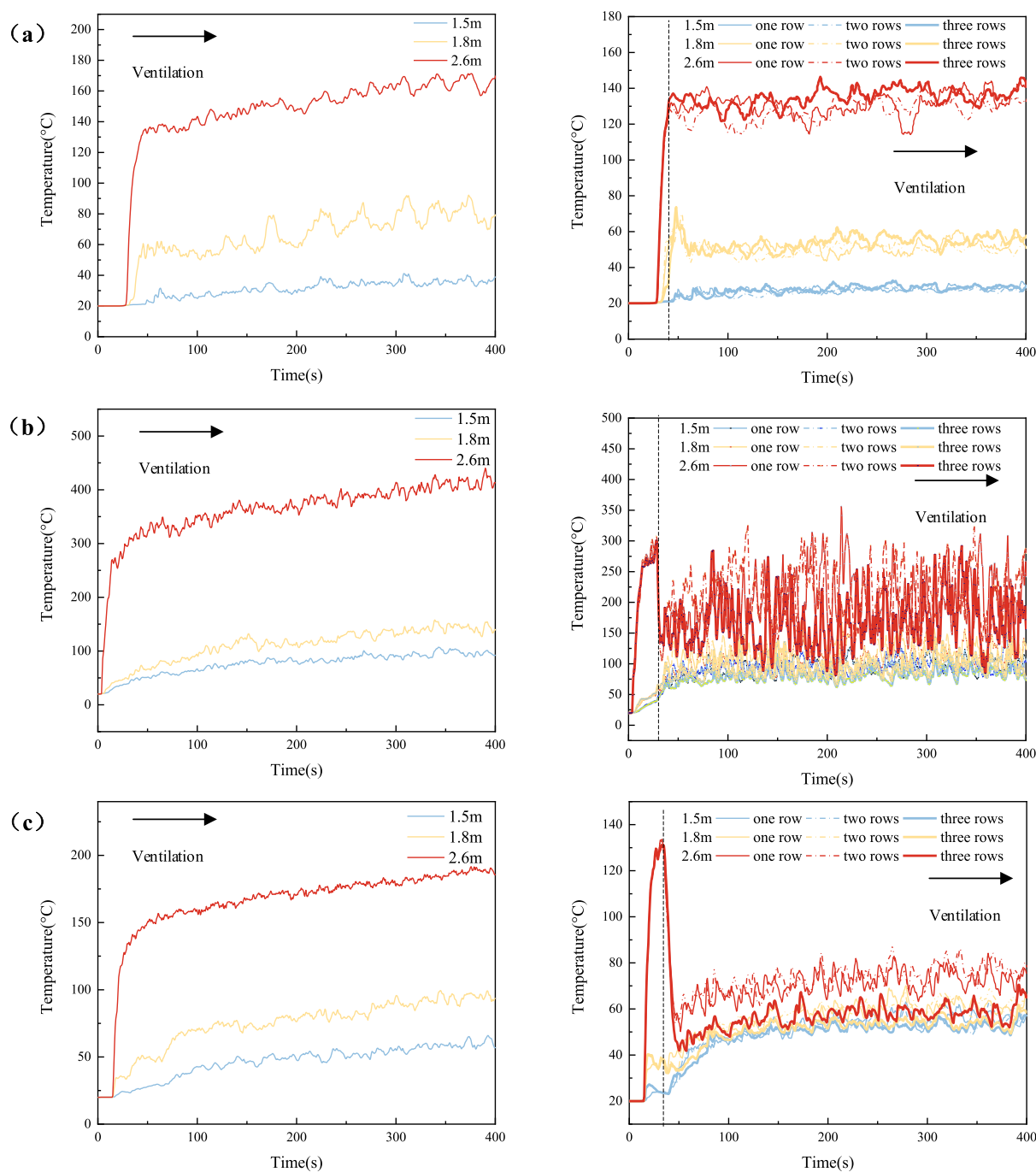


Figure 12. Quantitative comparison of simulation results at three heights for simulated systems with no spray (left) and systems with a water curtain system (right). (a) $Y = 1.5$ m, (b) $Y = 1.8$ m, and (c) $Y = 2.6$ m.

the fire stabilization phase (200–400 s). High CO concentrations are found in the area 1 m below the roof slab. The addition of the water curtain system reduced the stratification of CO concentrations near the fire source, resulting in CO concentrations in the tunnel of less than 0.03% (30 ppm).

Figure 17 depicts a change in CO concentration in the tunnel. Figure 16 shows the distribution of CO concentrations in the horizontal section at human eye height ($Y = 1.5$ m) during the fire stabilization period (200–400 s). The four cases found that CO concentrations in the area downstream of the fire source (50–100 m) increased with distance from the fire. When a water curtain system was added, the CO concentrations in (b), (c), and (d) decreased compared to the CO concentration in (a),

indicating that the water curtain system was also effective in preventing toxic gases. Figure 16b depicts the CO concentration change curve at $Z = 50$ m. The CO concentration can be seen to gradually increase throughout the simulation process. This is due to the fact that when the water curtain system is activated, the water vapor produced by the vaporization of the water mist droplets and the C cracked from the PVC form near the rubber surface. A large amount of CO was produced following the water gas reaction, causing the content to slowly increase, but its concentration downstream of the roadway was much lower than the evacuation standard 5×10^{-6} or 5 ppm.



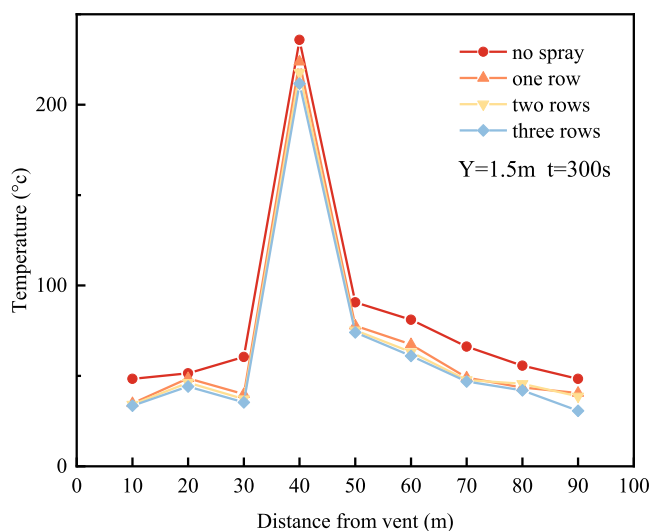


Figure 13. Numerical temperature distributions at 1.5 m above the floor level.

4. CONCLUSIONS

In this study, the effect of a water curtain system on a belt fire in an underground tunnel in a coal mine was investigated using CFD simulation. This study can provide guidance for the design, operation, and maintenance of smoke control in underground belt tunnels in coal mines. The main conclusions are as follows:

- (1) The installation of water curtain systems in underground tunnels is beneficial in creating a good evacuation and disaster avoidance environment for underground personnel and can effectively confine induced fires to the area between the water curtains. Ventilation speed affects the temperature distribution and the degree of fire control within the belt transport tunnel, and excessive mechanical ventilation speed can undermine the barrier effect of the water curtain system in underground tunnel fires. This study found that the mechanical ventilation speed should be controlled at approximately 0.8 m/s.
- (2) Observing the complex flow field in the tunnel, the plume close to the fire source bends the flow outward due to the obstruction of the longitudinal ventilation flow, carrying the hot smoke to the sidewalls of the tunnel and creating a temperature trough below the tunnel where the flow merges again into its center. In the vicinity of the water curtain system, the flow field around the fire source changes considerably, forming a plug shape. This was attributed to the blockage of flow caused by the water

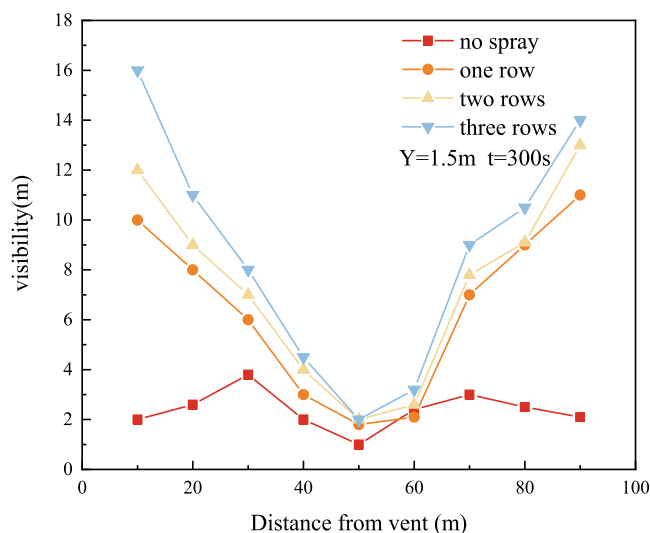


Figure 15. Numerical visibility distributions at 1.5 m above floor level.

curtain system, which affected the flow field around the fire source.

- (3) The presence of the water curtain system is more pronounced at the roof of the tunnel. The pushing effect of the airflow becomes increasingly apparent with increasing height, as shown in the temperature and velocity fields in the horizontal plane, with the blocking effect most evident at $Y = 2.6$ m. At the bottom of the tunnel, the airflow flows from left to right toward the water curtain, and the momentum of the water is blown away by the longitudinal airflow, causing hot flue gases to leak from the water spray area and attenuating the smoke blocking effect of the water curtain.
- (4) At a height of 1.5 m above the level of the human eye, the addition of a water curtain system will control the propagation of temperature and CO and rapidly regain visibility in the tunnel, despite the low visibility in the confined area between the water curtain system and the fire source. However, the temperature at 1.5 m above the tunnel floor is relatively low, at approximately room temperature level 30 °C, and the CO concentration is controlled to 20 ppm, which allows underground personnel to safely evacuate from the fire.

The water curtain system controls the propagation of smoke and temperature through the tunnel and is more flexible and has less effect on the tunnel structure than other physical compartment curtains, making it of greater research interest.

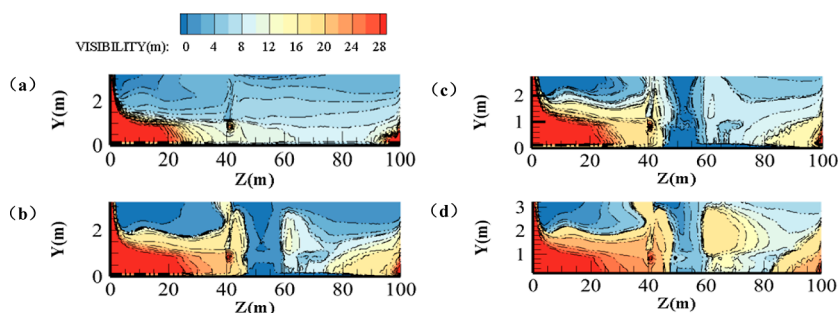


Figure 14. Visibility distribution in the tunnel. (a) No spray, (b) one row of water spray, (c) two rows of water spray, and (d) three rows of water spray. Values have been averaged over the steady-state period (200–400 s).

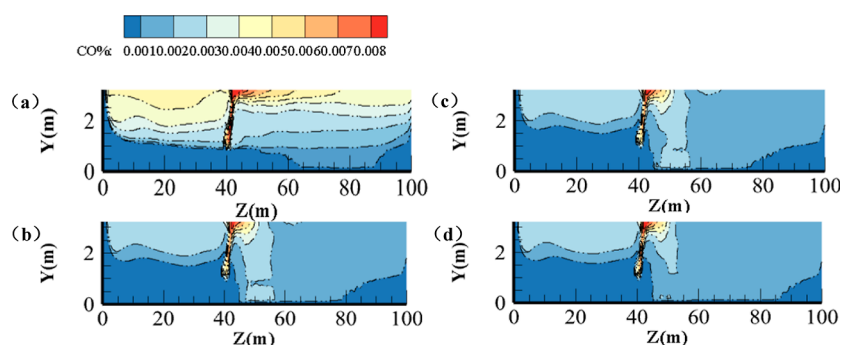


Figure 16. CO concentration distributions in the tunnel. (a) No spray; (b) one row of water spray; (c) two rows of water spray; and (d) three rows of water spray. Values have been averaged over the steady-state period (200–400 s).

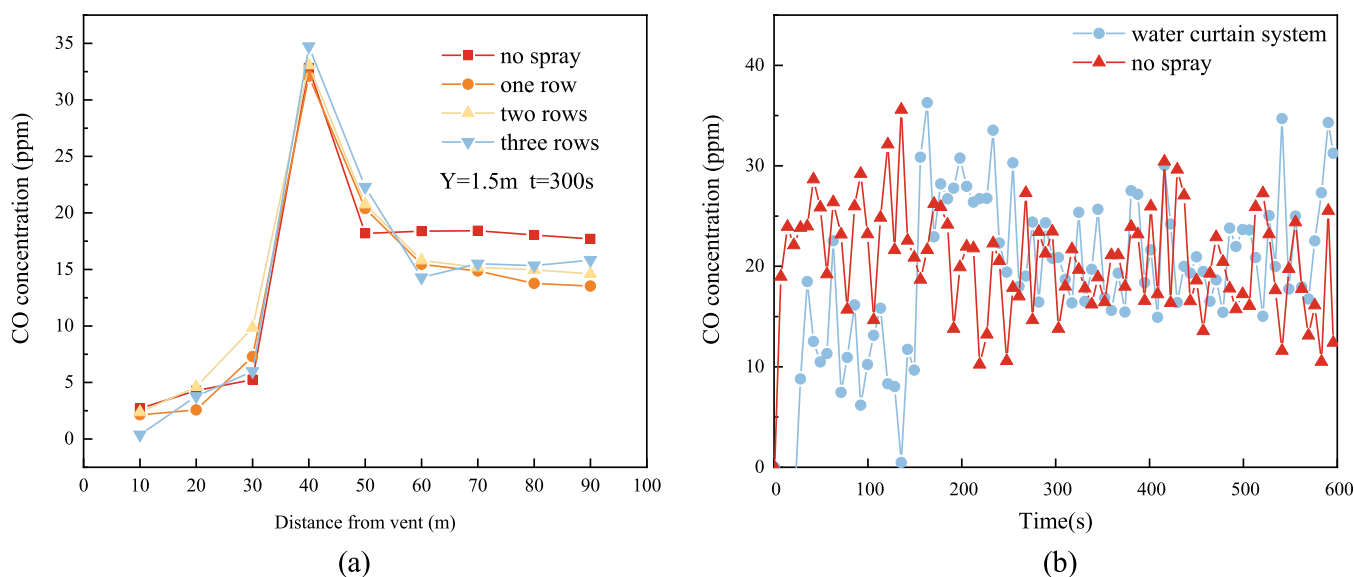


Figure 17. Numerical CO concentration distributions. (a) $Y = 1.5$ m and (b) $Z = 50$ m.

Little research has been carried out on this system in tunnels, so small-scale and full-scale combustion tests are needed in the future to give more confidence in its use in underground tunnel belt transport fires.

AUTHOR INFORMATION

Corresponding Authors

Jinzhong Jia – School of Safety Science and Engineering, Liaoning Technical University, Fuxin 123000 Liaoning, China; Key Laboratory of Mine Thermal Disaster and Prevention, Ministry of Education, Huludao 125000 Liaoning, China; orcid.org/0000-0002-4952-3318; Email: 525546192@qq.com

Guangbo Che – School of Safety Science and Engineering, Liaoning Technical University, Fuxin 123000 Liaoning, China; Key Laboratory of Mine Thermal Disaster and Prevention, Ministry of Education, Huludao 125000 Liaoning, China; Key Laboratory of Preparation and Applications of Environmental Friendly Materials (Jilin Normal University), Ministry of Education, Changchun 130103, P.R. China; Email: guangboche@jlnu.edu.cn

Author

Yinuo Chen – School of Safety Science and Engineering, Liaoning Technical University, Fuxin 123000 Liaoning, China; Key Laboratory of Mine Thermal Disaster and

Prevention, Ministry of Education, Huludao 125000 Liaoning, China

Complete contact information is available at:
<https://pubs.acs.org/10.1021/acsomega.2c05454>

Notes

The authors declare no competing financial interest.

ACKNOWLEDGMENTS

The work was supported by the National Natural Science Foundation of China (grant number 52174183).

REFERENCES

- (1) Barbato, L.; Cascetta, F.; Musto, M.; Rotondo, G. Fire safety investigation for road tunnel ventilation systems - An overview. *Tunn. Undergr. Space Technol.* **2014**, *43*, 253–265.
- (2) Brandies, J.; Bergmann, D. J. A numerical study of tunnel fires. *Combust. Sci. Technol.* **1983**, *35*, 133–155.
- (3) Chow, W. K. Experimental evaluation of the zone models CFAST, FAST and CCFM.VENTS. *J. Appl. Fire Sci.* **1992**, *02*, 307–332.
- (4) Chow, W. K. Simulation of tunnel fires using a zone model. *Tunn. Undergr. Space Technol.* **1996**, *11*, 221–236.
- (5) Hwang, C. C.; Wargo, J. D. Experimental study of thermally generated reverse stratified layers in a fire tunnel. *Combust. Flame* **1986**, *66*, 171–180.

- (6) Hu, L.; Fong, N.; Yang, L.; Chow, W.; Li, Y.; Huo, R. Modeling fire-induced smoke spread and carbon monoxide transportation in a long channel: fire dynamics simulator comparisons with measured data. *J. Hazard. Mater.* **2007a**, *140*, 293–298.
- (7) Hu, L.; Huo, R.; Wang, H.; Yang, R. Experimental and numerical studies on longitudinal smoke temperature distribution upstream and downstream from the fire in a road tunnel. *J. Fire Sci.* **2007b**, *25*, 23–43.
- (8) Hu, L.; Huo, R.; Chow, W. Studies on buoyancy-driven back-layering flow in tunnel fires. *Exp. Therm. Fluid Sci.* **2008a**, *32*, 1468–1483.
- (9) Hu, L.; Peng, W.; Huo, R. Critical wind velocity for arresting upwind gas and smoke dispersion induced by near-wall fire in a road tunnel. *J. Hazard. Mater.* **2008b**, *150*, 68–75.
- (10) Hu, L.; Tang, F.; Yang, D.; Liu, S.; Huo, R. Longitudinal distributions of CO concentration and difference with temperature field in a tunnel fire smoke flow. *Int. J. Heat Mass Tran.* **2010**, *53*, 2844–2855.
- (11) Fan, C.; Zhang, L.; Jiao, S.; Yang, Z.; Li, M.; Liu, X. Smoke spread characteristics inside a tunnel with natural ventilation under a strong environmental wind. *Tunn. Undergr. Space Technol.* **2018**, *82*, 99–110.
- (12) Amano, R.; Kurioka, H.; Kuwana, H.; Murakami, M.; Tsuruda, T.; Suzuki, T.; Ogawa, Y. Applicability of water screen fire disaster prevention system to road Tunnels in Japan. *3rd International Conference "Tunnel Safety and Ventilation"*; Graz University Of Technology: Graz, 2006; Vol. 03, pp 162–173.
- (13) Murakami, M.; Kurioka, H.; Imazeki, O.; Kuwana, H.; Amano, R. Numerical simulation in effect of compartmentalization with water screen in a tunnel fire. In *Underground Space- the 4th Dimension of Metropolises*; Barták, H., Romancov, Z., Eds.; CRC Press, 2007; Vol. 01, pp 1705–1710.
- (14) Ingason, H. Model scale tunnel tests with water spray. *Fire Saf. J.* **2008**, *43*, 512–528.
- (15) McCorry, T. Summary of water based fire safety systems in road tunnels and sub surface facilities. *Work Package 2.5 of the Research Project UPTUN of the European Commission (Revision 01) R250*; European Commission, 2008.
- (16) Liang, Q.; Li, Y.; Li, J.; Xu, H.; Li, K. Numerical studies on the smoke control by water mist screens with transverse ventilation in tunnel fires. *Tunn. Undergr. Space Technol.* **2017**, *64*, 177–183.
- (17) Sun, J. Y.; Fang, Z.; Tang, Z.; Beji, T.; Merci, B. Experimental study of the effectiveness of a water system in blocking fire-induced smoke and heat in reduced-scale tunnel tests. *Tunn. Undergr. Space Technol.* **2016**, *56*, 34–44.
- (18) Li, Q.; Tang, Z.; Fang, Z.; Yuan, J. P.; Wang, J. H. Experimental study of the effectiveness of a water mist segment system in blocking fire-induced smoke and heat in mid-scale tunnel tests. *Tunn. Undergr. Space Technol.* **2019**, *88*, 237–249.
- (19) Jiao, Z.; Yuan, S.; Ji, C.; Mannan, M. S.; Wang, Q. Optimization of dilution ventilation layout design in confined environments using Computational Fluid Dynamics (CFD). *J. Loss Prev. Process. Ind.* **2019**, *60*, 195–202.
- (20) Wang, W.; He, T.; Huang, W.; Shen, R.; Wang, Q. Optimization of switch modes of fully enclosed platform screen doors during emergency platform fires in underground metro station. *Tunn. Undergr. Space Technol.* **2018b**, *81*, 277–288.
- (21) Sakurahara, T.; Mohaghegh, Z.; Reihani, S.; Kee, E.; Brandyberry, M.; Rodgers, S. An integrated methodology for spatio-temporal incorporation of underlying failure mechanisms into fire probabilistic risk assessment of nuclear power plants. *Reliab. Eng. Syst. Saf.* **2018**, *169*, 242–257.
- (22) McGrattan, K.; Hostikka, S.; McDermott, R.; Floyd, J.; Weinschenk, C.; Overholt, K. *Fire Dynamics Simulator User's Guide*; NIST special publication, 2013.
- (23) McGrattan, K.; McDermott, R.; Hostikka, S. *Fire Dynamics Simulator (Version 6): User's Guide*; NIST Special Publication, 2017; Vol. 06, pp 1019–1025.
- (24) Chen, J.; Wang, J.; Wang, B.; Liu, R.; Wang, Q. An experimental study of visibility effect on evacuation speed on stairs. *Fire Saf. J.* **2018**, *96*, 189–202.
- (25) Gao, R.; Li, A.; Hao, X.; Lei, W.; Zhao, Y.; Deng, B. Fire-induced smoke control via hybrid ventilation in a huge transit terminal subway station. *Energy Build.* **2012**, *45*, 280–289.
- (26) Ji, J.; Zhong, W.; Gao, Z. *Smoke Movement and Control in Long and Narrow Spaces*; Science Press: Beijing, 2015.
- (27) Ji, J.; Guo, Y.; Gao, Z. H.; Zhu, J. P. Effects of ambient pressure on transport characteristics of thermal-driven smoke flow in a tunnel. *Int. J. Therm. Sci.* **2018**, *125*, 210–217.
- (28) Liu, R.; Jiang, D.; Shi, L. Agent-based simulation of alternative classroom evacuation scenarios. *Front. Archit. Res.* **2016**, *5*, 111–125.
- (29) Wang, W.; Zhu, Z.; Jiao, Z.; Mi, H.; Wang, Q. Characteristics of fire and smoke in the natural gas cabin of urban underground utility tunnels based on CFD simulations. *Tunn. Undergr. Space Technol.* **2021**, *109*, 103748.